

pubs.acs.org/est Article

Fostering a Holistic Understanding of the Full Volatility Spectrum of Organic Compounds from Benzene Series Precursors through Mechanistic Modeling

Dejia Yin, Bin Zhao,* Shuxiao Wang, Neil M. Donahue, Boyang Feng, Xing Chang, Qi Chen, Xi Cheng, Tengyu Liu, Chak K. Chan, Meredith Schervish, Zeqi Li, Yicong He, and Jiming Hao



Cite This: *Environ. Sci. Technol.* 2024, 58, 8380–8392



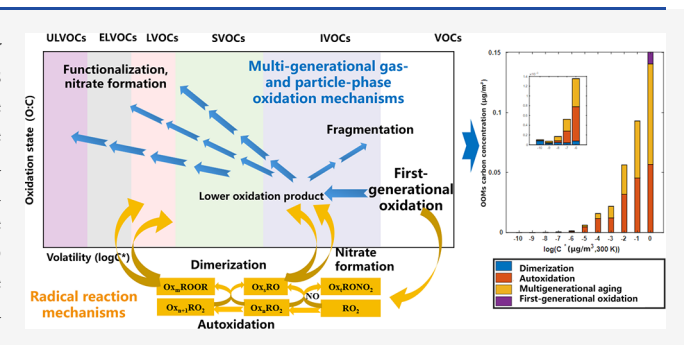
ACCESS I

III Metrics & More

Article Recommendations

Supporting Information

ABSTRACT: A comprehensive understanding of the full volatility spectrum of organic oxidation products from the benzene series precursors is important to quantify the air quality and climate effects of secondary organic aerosol (SOA) and new particle formation (NPF). However, current models fail to capture the full volatility spectrum due to the absence of important reaction pathways. Here, we develop a novel unified model framework, the integrated two-dimensional volatility basis set (I2D-VBS), to simulate the full volatility spectrum of products from benzene series precursors by simultaneously representing first-generational oxidation, multigenerational aging, autoxidation, dimerization,



nitrate formation, etc. The model successfully reproduces the volatility and O/C distributions of oxygenated organic molecules (OOMs) as well as the concentrations and the O/C of SOA over wide-ranging experimental conditions. In typical urban environments, autoxidation and multigenerational oxidation are the two main pathways for the formation of OOMs and SOA with similar contributions, but autoxidation contributes more to low-volatility products. NO_x can reduce about two-thirds of OOMs and SOA, and most of the extremely low-volatility products compared to clean conditions, by suppressing dimerization and autoxidation. The I2D-VBS facilitates a holistic understanding of full volatility product formation, which helps fill the large gap in the predictions of organic NPF, particle growth, and SOA formation.

KEYWORDS: full volatility spectrum of organic compounds, integrated two-dimensional volatility basis set, oxygenated organic molecules, secondary organic aerosol, benzene series precursors

1. INTRODUCTION

Aerosol particles play a key role in atmospheric pollution and have profound effects on human health and climate. New particle formation (NPF) is the main source of aerosol number concentration, and newly formed particles will contribute to cloud condensation nuclei (CCN) after growing above 50-100 nm, affecting the global climate by influencing the albedo and lifetime of clouds. 2-4 Condensation of organics is a main contributor to particle growth above 3 nm as well as secondary organic aerosol (SOA) concentration in both clean or polluted areas.⁵⁻⁸ Atmospheric organic compounds with different volatilities affect different stages of NPF and particle growth. Specifically, ultralow and extremely low-volatility organic compounds (ULVOCs and ELVOCs) can drive pure-organic nucleation and organic-H2SO4 nucleation, respectively, which is reported to be the major particle formation mechanisms in clean areas. 9,10 ULVOCs and ELVOCs also drive the initial growth of the newly formed particles. Low-volatility and semivolatile organic compounds (LVOCs and SVOCs) mainly drive the growth of larger particles and affect secondary organic aerosol (SOA) mass concentration by gas-particle-phase partitioning. Therefore, it is crucial to adequately simulate the full volatility spectrum of organic compounds, especially low-volatility compounds such as ULVOCs, ELVOCs, and LVOCs, with an integrated model in order to accurately quantify the environmental and climate effects of particles.

The low-volatility organics can be produced by the oxidation of volatile organic compound (VOC) precursors. The VOC precursors, on one hand, undergo regular multigenerational oxidation reactions induced by hydroxyl (OH), and, on the other hand, the peroxyl radicals (RO₂) from VOC precursors undergo irregular radical reactions like autoxidation, dimeriza-

Received: August 30, 2023 Revised: March 14, 2024 Accepted: April 18, 2024 Published: May 1, 2024





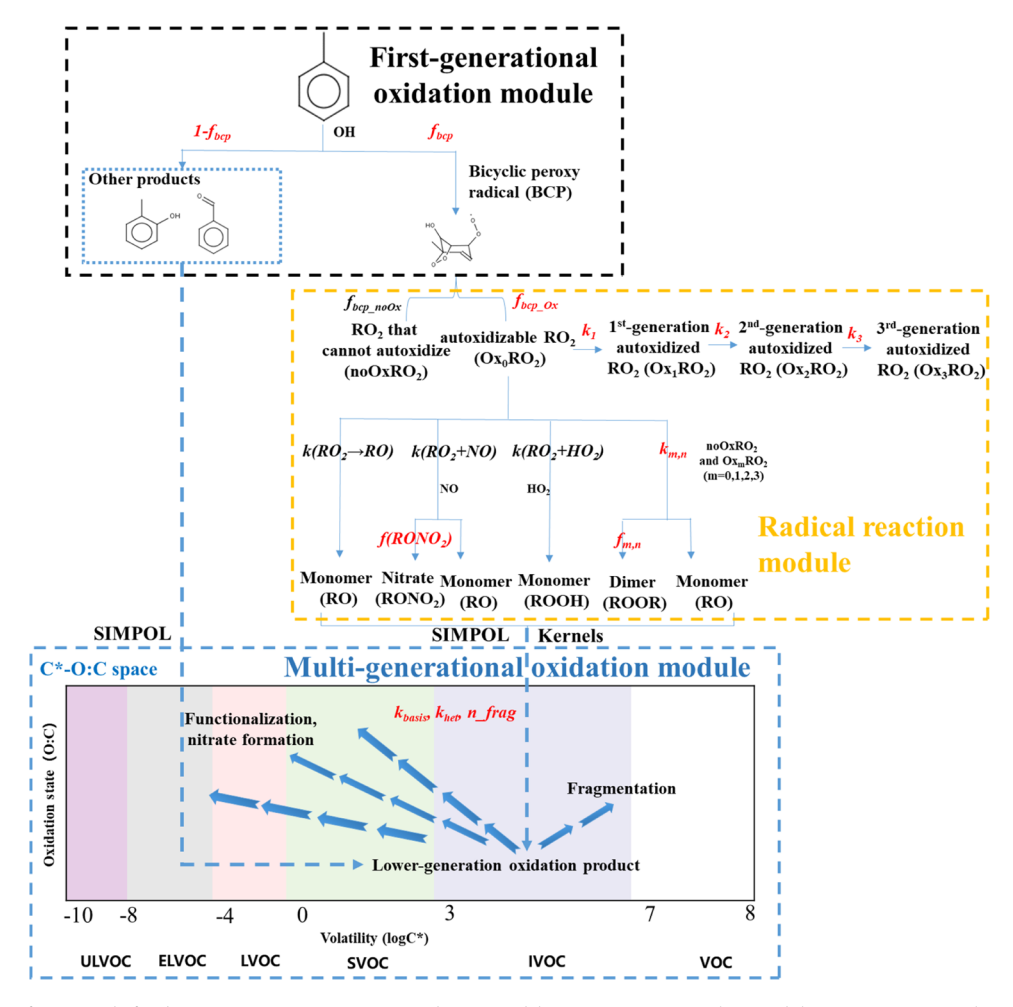


Figure 1. I2D-VBS framework for benzene series precursor oxidation and key parameters in the model. First-generational oxidation of benzene series VOCs is treated explicitly in the first-generation oxidation module, producing first-generation oxidation products, including bicyclic radicals. Radical reactions of bicyclic radicals are treated in the radical reaction module, with product volatility calculated based on SIMPOL. All products are distributed in the C^*-O/C space, and subsequent oxidation is treated via oxidation kernels in the multigenerational oxidation module.

tion, etc. ^{13,14} Oxidation products with low volatility and a high oxygen atom number are named oxygenated organic molecules (OOMs), which are potential driving factors of NPF and SOA formation. Earlier studies mainly focused on OOM formation from monoterpene in relatively clean areas. ^{15,16} In more polluted city areas, although monoterpene still contributed to OOM formation, ^{8,17,18} benzene series precursors, as important anthropogenic VOCs, have been recognized as a major contributor to OOMs in urban areas. ^{19,20} A few studies have shown that the growth rate of the newly formed particle can be largely explained by considering benzene series OOMs in some cities. ^{6,8} Furthermore, benzene series OOMs can contribute to 30–50% of SOA in several cities. ^{8,19} Hence, a holistic understanding of benzene series of OOMs in the full volatility range is vital in urban areas.

OOMs from the benzene series have been investigated by chamber experiments and theoretical calculations. The measurements of chamber experiments suggested that a large fraction of OOMs comprises products from bicyclic RO₂, ²¹, ²² which can undergo irregular radical reactions (autoxidation, dimerization, etc.). ²³ Experimental results with relatively high OH exposure also demonstrated the importance of multigenerational oxidation induced by OH, including functionalization and fragmentation, on benzene series OOM formation. ²⁴, ²⁵

Given the complexity of the benzene series oxidation chemistry, multiple major reaction pathways, including multigeneration oxidation and irregular radical reactions (autoxidation, dimerization, etc.), must be considered simultaneously to describe benzene series OOM formation precisely. Previous chemical mechanism models for benzene series compounds, such as SAPRC and carbon bond mechanism (CBM), can only represent the first few generations of oxidation based on empirical chamber fits. ^{26,27} The Master Chemistry Mechanism (MCM) model can simulate some of the multigenerational oxidation reactions at the expense of high computational cost, but many higher-generation oxidation reactions are still missing and irregular radical reactions (such as autoxidation and dimerization) involved in OOM formation have not been introduced into the model.²⁸ These models fail to simulate full volatility oxidation products from the benzene series compounds. The two-dimensional volatility basis set (2D-VBS) has been developed to represent multigenerational oxidation of various organic precursors.²⁹⁻³³ However, the traditional 2D-VBS model cannot simulate low-volatility products formed by irregular radical reactions. The radical 2D-VBS (R2D-VBS) was developed to simulate irregular radical reactions of monoterpene leading to OOM formation, 12,34 but multigenerational aging was not represented, which means R2D-VBS cannot reasonably depict the

formation of benzene series OOMs. 12,34 An integrated model that simultaneously represents the above-mentioned reaction pathways is urgently needed to reproduce the full volatility spectrum of products from benzene series precursors.

In this study, we developed an integrated 2D-VBS (I2D-VBS) model, simulating all major reaction pathways, including first-generation oxidation, multigeneration aging, and irregular radical reactions, within a unified framework. The parameterizations for benzene series compounds within I2D-VBS were determined initially by the literature and subsequently optimized by OOM and SOA experimental data. Compared with other models, this model framework can help describe the formation of oxidation products over the full volatility range quantitatively from VOC precursors and facilitate synchronous simulations of organic NPF, particle growth, and SOA formation. Finally, a series of simulations under typical urban conditions were conducted, and the effects of different pathways and environment conditions on benzene series of OOMs and SOA formation in the atmosphere are discussed.

2. METHODS

2.1. Development of the I2D-VBS Model Framework.

The I2D-VBS integrates multiple oxidation pathways and can simulate oxidation products over the full volatility range from benzene series compounds. It is comprised of three modules: first-generational oxidation module, radical reaction module, and multigenerational oxidation module. In Figure 1, the frameworks of the three modules and their main parameters are displayed.

2.1.1. First-Generational Oxidation Module. The firstgenerational oxidation module explicitly simulates the firstgeneration OH oxidation of benzene series precursors explicitly. O₃- and NO₃-initiated first-generational oxidation are not considered for their neglectable reaction rate constant compared to OH.35,36 The first-generational oxidation rates and products are mainly derived from the MCM model version 3.3.1,²⁸ and the yields of bicyclic peroxy radical (BCP, $f_{\rm bcp}$) are derived from chamber experimental results.^{37–40} We simulate radical reactions of BCP explicitly in the radical reaction module and define two kinds of RO2 for BCP: unautoxidizable RO₂ (noOxRO₂) and autoxidizable RO₂ (Ox₀RO₂). Yields of Ox_0RO_2 are defined as f_{bcp_Ox} and initially derived from theoretical calculations. There are three first-generational oxidation products of toluene other than bicyclic products in MCM, epoxide, cresol, and benzaldehyde. Some studies reveal that the fraction of the epoxide pathway is less than 0.01, 22,41,42 so we get rid of this pathway in the first-generational oxidation module compared to MCM. For cresol and benzaldehyde pathways, we trace their first-generation stable molecule products under low-NOx and high-NOx conditions based on MCM. 40 Considering cresol products have the potential to form bicyclic-like RO_2 , we adopt a higher f_{bcp} initial value within the possible ranges in Table S5 to represent this kind of products, while initial values of f_{cresol} and $f_{\text{benzaldehyde}}$ (yields of cresol and benzaldehyde) are smaller within the possible

2.1.2. Radical Reaction Module. In the radical reaction module, subsequent radical reactions of $noOxRO_2$ and Ox_0RO_2 are simulated. The parameters in the radical reaction module are initially derived from literature values (theoretical calculation, lab experiments, etc.). We assume that Ox_0RO_2 can undergo at most three generations of autoxidation $(Ox_1RO_2, Ox_2RO_2, Ox_3RO_2)$ because the oxygen numbers of

most RO2 and monomers detected in previous experiments^{23,44} were no more than 10. All RO₂ including noOxRO₂ can react with another RO2, HO2, and NO or undergo selftermination. The reaction rates of autoxidation are represented as k1, k2, and k3 (collectively named k_{auto}) (Table S5). Initial values and the temperature dependence of $k1 = \exp(9.67 -$ 3920/T) are obtained from the theoretical calculation by Wang et al., and k2 and k3 are estimated by a quasi-steady approximation based on experimental data in the same work.²³ We assume that k1, k2, and k3 have the same temperature dependence. $k_{m,n}$ (collectively named as k_{dimer}), $k(\text{RO}_2 + \text{HO}_2)$, and $k(RO_2 + NO)$ are the reaction rates of RO_2 with another RO_2 , HO_2 , and NO_2 , respectively (Table S5). $k_{m,n}$ represents the reaction rate between Ox_mRO_2 and Ox_nRO_2 (noOxRO₂ are also considered, m,n = 0,1,2,3) (Table S5). Cross-reactions between RO2 produce dimers (ROOR) or alkoxy radicals (RO). The fractions of dimer formation are expressed as $f_{m,n}$ (collectively named as f_{dimer}). The reaction between RO₂ and NO produces nitrate (RONO₂) and RO, and the fraction of RONO₂ formation is $f(RONO_2)$. Initial values of $k_{0.0}$ and $f_{0.0}$ are obtained from kinetic experiments. 43 Experiments showed that the formation rates of high oxygen-containing dimers are higher than those of low oxygen-containing dimers, which means Ox₁RO₂, Ox₂RO₂, and Ox₃RO₂ are more likely to dimerize compared with Ox_0RO_2 . Therefore, other k_{dimer} and f_{dimer} are assumed to be relatively larger than $k_{0,0}$ and $f_{0,0}$. The initial values of $k(RO_2 + HO_2)$ and $k(RO_2 + NO)$ are derived from kinetic results and former modeling research. 12,45 The value of $f(RONO_2)$ has large uncertainties in various studies $^{22,45-49}$ and can vary from 0 to 0.3, so its initial value is assumed to be 0.15.47 Stable molecules from radical reactions (i.e., ROOH, ROOR, and RONO2) are distributed into the two-dimensional (2D) space defined by log C* (calculated by the SIMPOL model) and O/C. RO radicals undergo functionalization and fragmentation and are also distributed into the 2D space. These products are categorized into three kinds: ROOH and stabilized RO products are monomer (also named non-nitrogenous monomer), ROOR is dimer, and RONO2 is nitrate. According to experimental results, the autoxidation rate of polysubstituted benzene series compounds may be larger than monosubstituted benzene series compounds by 1 order of magnitude, ^{23,44,47} so all of RO₂ (noOxRO₂ and Ox_mRO₂, m = 0,1,2,3) are separated into two kinds in the model and collectively defined as ARO2 and BRO₂, representing RO₂ from mono- and polysubstituted benzene series compounds, respectively. The autoxidation and dimerization parameters (k_{auto} , k_{dimer} , and f_{dimer}) of ARO₂ and BRO₂ are different. Details of radical reactions, their products, initial values of radical reaction parameters, and methods to distribute these products into the 2D space are described in Section S1 and Table S3. We also conduct a sensitivity simulation to demonstrate that the first-generational oxidation module and radical reaction module are necessary for reproducing full volatility product yields, especially lowvolatility products (see Section S2).

2.1.3. Multigenerational Oxidation Module. In the multigenerational oxidation module, products distributed into the 2D space undergo gas- and particle-phase multigenerational oxidation. The parameters in the multigenerational oxidation module are initially obtained from previous studies. 31,32,50 Vapor- and particle-phase aging rates are relevant to vapor- or particle-phase organics and OH concentrations, and their rate constants are k_{basis} and k_{het} (initial values are 2.5 and 3×10^{-11}

cm3 molecule-1 s-1, respectively). For functionalization, we assume that each step will reduce the $\log C^*$ by 1–7 orders of magnitude and add 1-3 oxygen atoms, consistent with the average addition of one -OH or one =O group per functionalization step. For fragmentation, we assume that carbon bonds in molecules break randomly and that radicals from broken molecules will undergo functionalization to form stable molecules. These assumptions on product distributions in the 2D space are represented by matrices named "kernels" (Tfunc and Tfrag in Tables S1 and S2). The fraction of fragmentation is $(O:C)^{n_{\text{frag}}}$ (see n_{frag} in Table S5). When NO_x exists, multigenerational oxidation products can be nitrate or non-nitrogenous products. The branching ratio of nitrate products of multigenerational oxidation (β in Table S5) is calculated by the ratio of NO_x and precursor concentration. Gas-particle partitioning and wall loss are also considered. The initial values of k_{basis} , k_{het} and n_{frag} are derived from our previous studies. 30,32

A specific mathematical overview of I2D-VBS and methods for determining the initial values of model parameters is displayed in Section S1. Although the initial parameters are determined from the literature, they can be adjusted within a reasonable range. This is because only a few parameters are measured directly by kinetic experiments, such as the dimerization rate of Ox₀RO₂, while other parameters are either derived from theoretical calculations or deduced from similar experiments or theoretical calculation results. Furthermore, some measured parameters have large differences between various studies. For example, the dimer formation rate of Ox₀RO₂ in various studies can vary from $\sim 10^{-12}$ to $\sim 10^{-10}$ cm³ molecule⁻¹ s⁻¹. ^{28,43} In addition, parameters in the model represent the average characteristics (reaction rate, branching ratio, etc.) of a group of reactions and not the characteristics of a specific reaction. Consequently, it is justified to optimize the values of the parameters within a reasonable range (determined from previous studies; see Table S5) by simulating laboratory experiments so that the simulation results match well with OOM and SOA measurements. Because there are many parameters in the three modules, synchronous optimization of all parameters is difficult. Hence, we use a stepwise strategy that successively optimizes parameters in different modules with different experiments. The detailed optimization steps are shown in Section 3.2.

2.2. Simulations of Laboratory Experiments Measuring OOMs and SOA from Benzene Series Oxidation. 2.2.1. Laboratory Experiments Used in This Work. To optimize parameters in the model, we simulate laboratory experiments measuring OOMs and SOA. Chemical ionization mass spectrometers (CIMS) can measure OOMs at the molecular level, which provides detailed information about volatility, oxidation state, and crucial molecular components of the OOMs. Experiments measuring OOMs used in this work were conducted by Molteni et al.44 and Cheng et al.24 Experiments conducted by Molteni et al. cover various benzene series precursors, including toluene, ethylbenzene, mesitylene, and xylene, with a relatively low OH exposure (4.5 \times 10⁹ cm⁻³·s, equivalent to 0.8 h if assuming the average ambient OH concentration is $1.5 \times 10^6 \text{ cm}^{-3}$)^{SY} and without NOx. Cheng et al. reported experiments on toluene, with a higher OH exposure ($\sim 2.2 \times 10^{11}$ cm⁻³·s, equivalent to 1.70 days) than Molteni et al. over a range of NO_x concentrations (0 or 200 ppb, denoted as low NO_x and high NO_x). The effects of wall losses and OOM condensation on the particle

phase have been considered in the studies of Molteni et al. and Cheng et al., 24,44 following the methods described in Section S3. Experiments measuring the SOA used in this work include those conducted in the oxidation flow reactor (OFR) and environmental chamber. We conducted a series of OFR experiments with low (55.3 ppb) and high (268.2 ppb) toluene concentrations without NO,, and the OH exposure range is $0.2-8.8 \times 10^{11} \text{ #/cm}^3 \cdot \text{s}$ (equivalent to 0.2-6.8 days). More experimental details are shown in Section S4. Another OFR experiment of toluene without NOx conducted by Liu et al. is also simulated in this work, with an initial toluene concentration of 138 ppb and an OH exposure range of $0.5-5.2\times10^{11}~cm^{-3}$ ·s (equivalent to 0.4–4.0 days). 52 Chamber experiments of toluene are conducted by Ruiz et al., 53 with high-NO_x concentration (about 1000 ppb) and an equivalent aging time of 1.85 days (real reaction time of 7 h). Particle wall losses have been corrected in the experiments measuring SOA, and vapor wall losses are simulated by formula in Section S1, and the wall loss rates are estimated following previous studies. 54,55 The experiments cover a wide range of precursor concentrations (50-800 ppb), OH exposure (4 × $10^8-8 \times 10^{11}$ cm⁻³·s), and NO_x concentrations (0–1000 ppb).

2.2.2. Comparison Method between Simulations and Measurements. We mainly compare simulated and measured OOM carbon yields in volatility and O/C dimensions. The measurements of OOMs only provide molecular formula and concentrations but cannot provide the volatility directly, so the volatility of observed products is usually estimated by molecular formula. We propose a volatility estimation method by combining empirical formulas of other studies^{21,25,29} and linear fitting using SIMPOL. Specific details of volatility estimation are shown in Section S5. Normalized mean biases (NMBs) of the OOM carbon yields, SOA concentration/ yields, and the O/C ratios are calculated to quantify the simulation biases. The specific calculation method of NMB is shown in Section S6. For the NMB calculation of OOM carbon yields of the carbons of the OOMs, we take the sensitivity of the detection instruments into consideration. Ideally, we would compare all products, but some products with lower oxygen numbers and higher volatility can only be partly detected by NO₃-CIMS, which are not compared with simulated yields directly. We only include OOM carbon yields of the easily detected products of the OOMs in a specific volatility and the O/C range (log $C^* \le -1$, O/C ≥ 0.6 for the non-nitrogenous monomer and nitrate and log $C^* \leq -2$, O/C ≥ 0.3 for the dimer) when calculating NMB. We classify the products as unautoxidized (Ox₀) products, first-generation autoxidized (Ox₁) products, second-generation autoxidized (Ox_2) products, and third-autoxidized (Ox_3) products by autoxidation generations and distinguish the easily and partly detected products among them. The differentiation of easily and partly detected products is shown in Section S6. According to previous studies, the uncertainty ranges of OOM concentrations detected by NO₃⁻-CIMS can be -50-100%; hence, we regard -0.5-1 as an acceptable range for NMB. 56,57 Since the high-volatility products are only partly detected by NO₃-CIMS, we also allow simulated carbon yields of products with higher volatility to be higher than measurements so that the simulated low-volatility products match measured data. For example, assuming two cases with similar NMB, if total yields of simulated oxidation products are higher than measured yields, but yields of low volatility can match

measured data in one case, and total yields of simulated oxidation products can match measurement, but yields in low volatility are lower than measured data in another case, we regard the former case as more acceptable. For the experiments of Molteni et al.,⁴⁴ we also distinguish generations of autoxidation of measured products and compare them with simulated autoxidized products, and the details are shown in Section S7. For experiments measuring SOA, the NMBs of SOA concentrations/yields and O/C are expected to be much lower than those of the OOMs.

3. RESULTS AND DISCUSSION

3.1. Laboratory Experiment Simulations Using the Initial I2D-VBS Parameterizations. We simulate experiments measuring the OOMs and SOA with initial parameters determined from the kinetic literature (theoretical calculation, lab experiments, etc.; see Section 2.1). OOMs and SOA simulations are shown in Figures S1 and S2, and the NMBs of OOM carbon yields of the OOMs, SOA yields, and O:C are shown in Table S6. For experiments of Molteni et al., 44 NMB values of monomers and dimers range from -0.58 to -0.91 for the precursors considered. For low-NO_x experiments of Cheng et al., 24 the NMB of monomers is -0.40 and that of dimers is -0.47, with NMB absolute values lower than those of Molteni et al.44 In high-NOx experiments of Cheng et al.,24 the simulated yields of nitrates are reasonable (NMB = -0.27), but non-nitrogenous monomers are highly underestimated (NMB = -0.97). In summary, the initial parameters generally underestimate OOM formation. Simulated SOA mass yields are higher (NMB > 1.9) and O/C is lower (NMB \leftarrow 0.3) than measured values in low-NO_x OFR experiments conducted in this work and by Liu et al., 52 while simulated SOA and O/C in high-NO_x experiments by Ruiz et al.⁵³ agree with experimental data well (absolute NMB < 0.10). The results reveal that the model can capture SOA formation in high-NO, conditions but have a non-negligible bias in low-NO_x conditions.

The initial parameters may underestimate the level of OOM formation because either autoxidation or multigenerational oxidation is underestimated; this should be identified. Molteni et al.44 and Cheng et al.24 attribute major products detected in their experiments to ring-retaining products because their C numbers are close to the C number of precursors and H and O numbers are similar to bicyclic products, which means these products probably retain the bicyclic structure. From the H and O numbers of these products, we can determine their main formation pathways. In the experiments of Molteni et al., 44 the mass spectrum showed a sequence of ring-retaining product peaks separated by a mass corresponding to two oxygen atoms, which may be attributed to O2 addition caused by autoxidation. 44 Additionally, the low OH exposure and short reaction time in the experiments of Molteni et al. 44 result in weak multigenerational aging, which corroborates that the O2 addition during OOM formation is probably attributed to autoxidation. In the experiments of Cheng et al., 24 OOM species with 1 or 2 oxygen number difference can be detected, which may involve multiple pathways (autoxidation and multigeneration oxidation).²⁴ The H number in the measured molecules can help identify multigenerational oxidation products. If the H number of a ring-retaining molecule is less than the H number of the precursor (y) or larger than y +2, the molecule is regarded as having undergone H abstraction or OH addition (the first step of oxidation by OH), respectively.²⁴ Concentrations of these products are indeed

found to be correlated with the OH concentration. However, the remaining ring-retaining products ($y \le H$ number $\le y + 2$), which are much more abundant, show little correlation with OH, indicating that these products are probably not all multigenerational products (Figure 3 in Cheng et al.²⁴). From the molecular observation results, it seems that autoxidation is significant in these two experiments. We also turned off autoxidation pathways in our simulations using initial parameters to confirm the importance of autoxidation, whose results are shown in Figure S3. Obviously, simulating only multigenerational oxidation products cannot reproduce the formation of OOMs, especially the low-volatility products. Thus, most of the OOMs in the experiments of Molteni et al. 44 and part of the OOMs in the experiments of Cheng et al.²⁴ should be explained by autoxidation. Based on the analysis of molecular observations and sensitivity simulations, k_{auto} in the initial parameters is likely underestimated. For dimerization, less autoxidized RO2 due to the previously discussed poor representation of autoxidation and underestimation of k_{dimer} and f_{dimer} by initial parameters are all possible reasons for dimer underestimation, so we will further diagnose the biases after k_{auto} is adjusted in the next section.

3.2. Optimized I2D-VBS Parameterization and Updated Simulation Results. The simulation results of the initial parameterization have systematic bias compared with measured results, and parameters should be optimized to achieve better model-measurement agreement according to Section 2.1. We adopt a stepwise optimization method to optimize model parameters, ensuring efficiency and clarity. This method significantly reduces the complexity of parameter optimization and facilitates an understanding of how each free parameter impacts the SOA simulations. While there are multiparameter optimization frameworks available to simultaneously tune multiple parameters, 58,59 offering more comprehensive optimization outcomes, due to the specific characteristics and complexity of our model, as well as the existing knowledge we have gained from the simulation results corresponding to the initial parameters in Section 3.1, a more efficient stepwise optimization approach might already be sufficient here. In the experiments of Molteni et al., 44 most of the oxygenated products detected by nitrate-CIMS should be explained by autoxidation and dimerization. So, experiments of Molteni et al. 44 are used to constrain k_{auto} , k_{dimer} , and f_{dimer} in the first step. From Section 3.1, k_{auto} should be higher than the initial parameters. After we increase k_{auto} by 8–30 times (8 for monosubstituted benzene series species and 30 for polysubstituted species, both within the reasonable range determined from the literature) and guarantee that the non-nitrogenous monomer can match measured data, dimer yields are 2-4 times those of measurements (2-10 times for dimers in specific volatility ranges). Hence, we lower $k_{\rm dimer}$ by 2–10 times and f_{dimer} by 2 times (except for $f_{0,0}$) according to measured dimer concentrations. Ox₀ROOR is only partly detected by NO_3^- -CIMS, so $f_{0.0}$ cannot be determined by measured OOM yields. However, the formation of Ox₀ROOR largely increases the concentration and decreases the O/C of SOA; hence, $f_{0.0}$ can be determined by experiments measuring SOA. After adjusting k_{auto} , k_{dimer} , and f_{dimer} except for $f_{0,0}$, we simulate experiments measuring OOMs by Cheng et al.²⁴ and those measuring SOA to optimize parameters in the multigenerational module and $f_{0,0}$. For the parameters in multigenerational oxidation module, the optimization is based on the influence of parameters in this module on SOA

concentrations and O/C, which has been discussed in previous studies. 31,32,50 After the two-step optimization, we resimulate all experiments with optimized parameters to confirm their suitability. The optimized parameters are shown in Table S5, and the important parameters in Figure 1 are shown in Table 1.

Table 1. Optimized Values of Important Parameters in I2D-VBS Model

parameters		optimized value
branching ratio of 1st-generation products	$f_{ m bcp}$	0.67 (toluene)
		0.67 (ethylbenzene)
		0.73 (mesitylene)
		0.73 (xylene)
	$f_{ m bcp_Ox}$	0.07 (toluene)
		0.12 (ethylbenzene)
		0.20 (mesitylene)
		0.18 (xylene)
	$f_{ m cresol}$	0.26 (toluene)
		0.26 (ethylbenzene)
		0.20 (mesitylene)
		0.20 (xylene)
	$f_{ m benzaldehyde}$	0.07 (toluene)
	, ,	0.07 (ethylbenzene)
		0.07 (mesitylene)
		0.07 (xylene)
autoxidation rate (s ⁻¹)	<i>k</i> 1	$\exp(9.67 - 3920/T) \times 8$ (ARO ₂)
		$\exp(9.67 - 3920/T) \times 30$ (BRO ₂)
	k2	$k1/0.42/4 \text{ (ARO}_2)$
		k1/0.42/10 (BRO ₂)
	k3	$k2/1.3 \text{ (ARO}_2)$
		$k2/1.3/2 (BRO_2)$
	1.00	$2.8/4 \times 10^{-10} (ARO_2)$
	k00	$2.8/2 \times 10^{-10} (BRO_2)$
	k11	$4.9/8 \times 10^{-10} (ARO_2)$
dimerization rate		$4.9/2 \times 10^{-10} (BRO_2)$
$(k_{m,n} = \sqrt{k_{mm}k_{nn}})$, units: cm ³ molecule ⁻¹ s ⁻¹	k22	$8.7/2 \times 10^{-10} (ARO_2)$
		$8.7/5 \times 10^{-10} (BRO_2)$
	k33	$8.7/2 \times 10^{-10} (ARO_2)$
		$8.7/10 \times 10^{-10} (BRO_2)$
dimerization fraction (where $n = 1,2,3$)	$f_{0,0}$	0.015 (ARO ₂)
		0.015 (BRO ₂)
	$f_{0,n}$	0.5 (ARO ₂)
	J - J	0.25 (BRO ₂)
	$f_{n,n}$	0.5 (ARO ₂)
	J 11,111	0.25 (BRO ₂)
$k(RO_2 + HO_2)$ (cm ³ molecule ⁻¹ s ⁻¹)		1×10^{-11}
$k(RO_2 + NO)$ (cm ³ molecule ⁻¹ s ⁻¹)		1×10^{-11}
$f(RONO_2)$		0.15
$k(RO_2 \rightarrow RO) (s^{-1})$		$10^{15} \times \exp(-13,000/T)$
k_{basis} (cm ³ molecule ⁻¹ s ⁻¹)		2.5×10^{-11}
$k_{\text{het}} \text{ (cm}^3 \text{ molecule}^{-1} \text{ s}^{-1}\text{)}$		3×10^{-12}
n frag		0.3

The simulation and observation of OOM carbon yields by volatility bins based on optimized parameters are shown in Figure 2. For the experiments of Molteni et al.,⁴⁴ simulated yields of low-volatility ($\log C^* \le -1$ for non-nitrogenous monomers and nitrates and $\log C^* \le -2$ for dimers) agree reasonably well with measurements (NMB values are within -0.5-1, with most of NMB values within -0.3-0.6). For the

low-NO $_x$ experiments of Cheng et al., ²⁴ the NMB values are within ± 0.3 and the fractions of autoxidized products are higher than those simulated using the initial parameters (from lower than 1 to ~10%), which shows good consistency with the analysis of Cheng et al. ²⁴ For high-NO $_x$ experiments, the trend of decreasing nitrate concentration with decreasing volatility can be reproduced fairly well. For non-nitrogenous monomers, simulated yields of autoxidized products are lower than measured OOM yields, but if Ox $_0$ monomers are added, the simulated yields are higher than observed. Considering Ox $_0$ non-nitrogenous monomers (mainly formed by RO from RO $_2$ + NO reactions) are only partly detected by NO $_3$ --CIMS, the simulation yields of non-nitrogenous monomers are deemed acceptable.

We also compared the simulated O/C of OOMs with experiments, and the results are shown in Figure S4. Here, NMBs are still calculated based on non-nitrogenous monomers and nitrates with $\log C^* \le -1$ and dimer with $\log C^* \le -2$, so the NMB values of each experiment are the same as those reported above. In the experiments of Molteni et al.⁴⁴ and Cheng et al.,²⁴ our model generally reproduces the observed trend that OOM yields first increase and then decrease with the increase of O/C. However, there are still biases on volatility and O/C distributions of OOMs between simulations and measurements for some individual experiments due to the uncertainty of distribution kernels of radical reaction products, which have been discussed in Section S8. This kind of bias is acceptable under low OH concentration and can be ignored under high OH conditions. We also compare the yields of monomers and dimers with different generations of autoxidation, and the simulated yields can agree with measured yields within acceptable biases (details are shown in Section S7 and Figure S5).

Experiments measuring SOA are also simulated by the optimized parameters. Simulation results of chamber experiments by Hildebrandt Ruiz et al.⁵³ and OFR experiments conducted in this work with low toluene concentration (whose precursor concentrations are closer to ambient conditions than the high-toluene OFR experiments) are shown in Figure S6. The NMB values of the O/C and SOA concentrations of the two experiments are within ± 0.10 , showing the model's ability to simulate the SOA formation and oxidation state under different oxidant exposures. Compared to simulations using the initial parameters, the optimized parameters can better reproduce the trends that SOA yields first increase and then decrease while O/C keeps increasing with the increase of OH exposure in both low- and high-NO_x conditions. Simulation results of other experiments measuring SOA are also shown in Figure S6. For high-toluene OFR experiments conducted in this work, simulated SOA concentrations are higher than observed at long oxidation equivalent time (NMB = 0.12), while the NMB of the O/C is small (0.03). The overestimation of SOA concentration is probably because the strong UV exposure (as indicated by a high O₃ concentration of >30 ppm in the reactor) might induce fierce SOA photolysis, which is not considered in the model. 60,61 For the experiments of Liu et al., 52 the O/C is overestimated (NMB = 0.48), and the NMB of SOA is 0.03, but the variation of O/C and SOA yields with OH exposure agrees with the measurements. Overall, the model captures the distribution of OOM products in terms of volatility and O/C reasonably well under various experimental conditions, while concentration, oxidation state, and time variation of SOA can also be reproduced reasonably, which

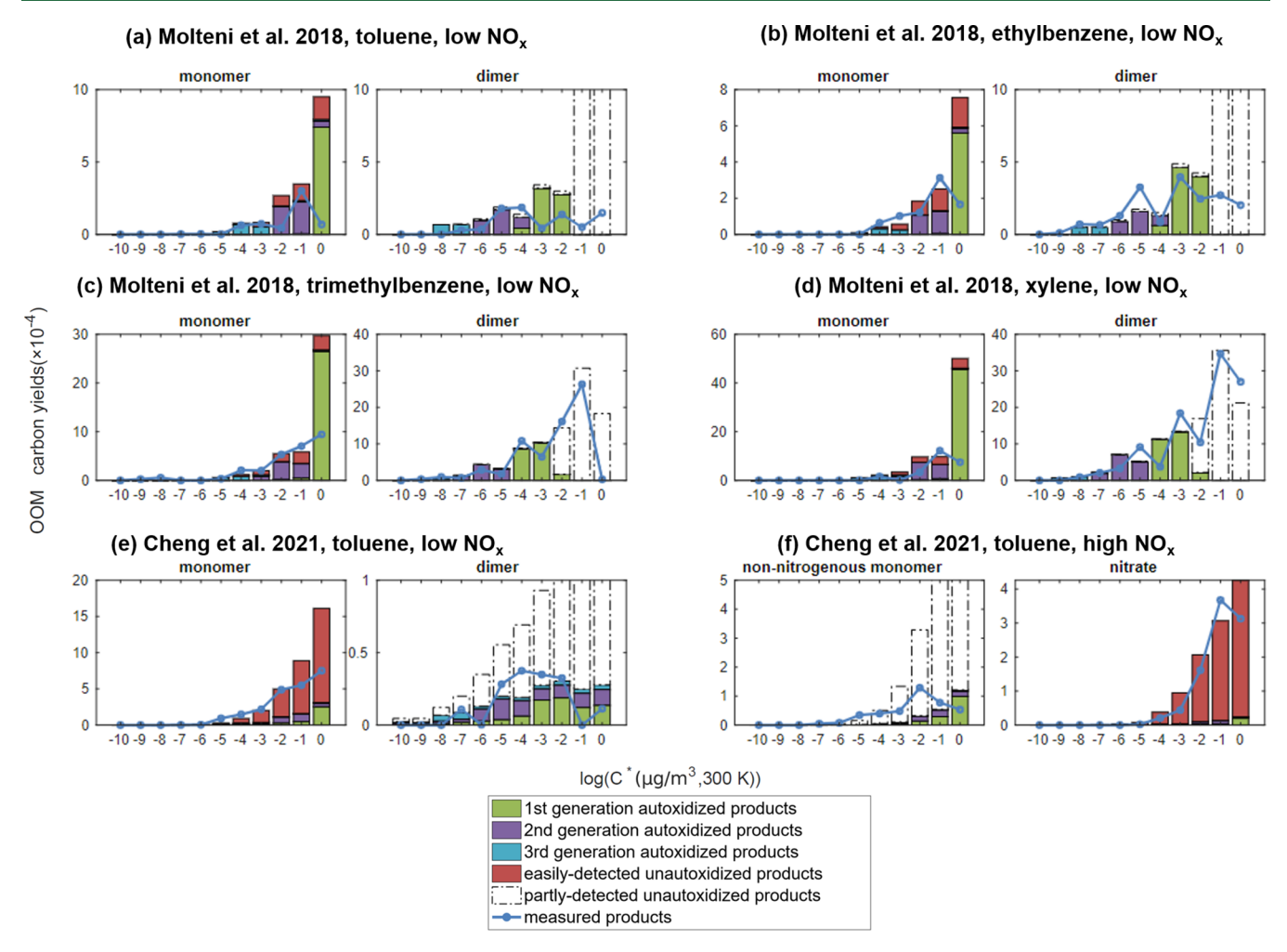


Figure 2. Comparison of simulated carbon yields of benzene series oxidation products with measured yields of OOMs in the (a) toluene, (b) ethylbenzene, (c) trimethylbenzene, and (d) xylene experiments conducted by Molteni et al. ⁴⁴ in low- NO_x condition and the toluene experiments by Cheng et al. ²⁴ in (e) low and (f) high- NO_x conditions. Both simulated and measured yields are bound by volatility. Simulated yields of the low-volatility products can match observed values, while we allow simulated yields of high-volatility products to be higher than observed considering the lower sensitivity of NO_3 -CIMS to these products.

demonstrates the ability of the model to simulate and quantify the formation of products over the full volatility simultaneously.

To guarantee the accuracy of optimized parameters, we also design several sensitivity cases for main parameters in the three modules, including $f_{\rm bcp}$ in the first-generation oxidation module, k_{auto} , k_{dimer} , f_{dimer} , and $f(\text{RONO}_2)$ in the radical reaction module, and \vec{k}_{basis} and n_{frag} in the multigenerational oxidation module. The details are listed in Section S9. The sensitivity analysis demonstrates that the optimized parameters can better match lab experiments compared to the sensitivity cases and that the assumptions of the model are reasonable. Owing to available measurements of OOMs and SOA, all of the parameters can be confined to relatively smaller ranges than those in literature ranges. Although the parameters in the three modules are demonstrated as the most reasonable scheme by sensitivity analysis, some parameters need further verification in future studies due to the lack of experimental data or the uncertainty in existing experiments. According to the sensitivity analysis, k_{auto} has comparatively large impacts on OOM yields and its values span a wide range in the literature; thus, direct measurements of k_{auto} in future studies would be valuable for the verification and further optimization of the

parameters used in the model. In addition, $f(RONO_2)$ values of different RO_2 should be different, but due to the lack of experimental results, we assume a uniform $f(RONO_2)$ for all RO_2 , which would bring uncertainty to the OOMs and SOA simulation in high- NO_x conditions. Moreover, the current I2D-VBS model has not considered some reaction pathways explicitly, including the autoxidation of nonbicyclic RO_2 from isomerization of bicyclic RO_2 radicals, $\frac{22,48,49}{2}$ due to the lack of measurements of their kinetic parameters, which also requires further exploration in future studies.

3.3. Simulation of OOMs and SOA Formation under Typical Urban Conditions. We design simulations under typical urban conditions to investigate the full volatility spectrum of products from benzene series precursors in the atmosphere and to evaluate contributions of different pathways and the effects of atmospheric conditions. Because benzene series precursors are a major source of SOA and OOMs in urban areas, 6,19 we simulate the conditions of a typical polluted city, Beijing. The concentrations of precursors (8.5 ppb in total), OH (1.5 × 10⁶ #/cm³), and NO_x (10 ppb), as well as the temperature (300 K) and reaction time (6 h) of the base case, are determined from previous studies. 62,63 We also design sensitivity cases to discuss the effect of different reaction

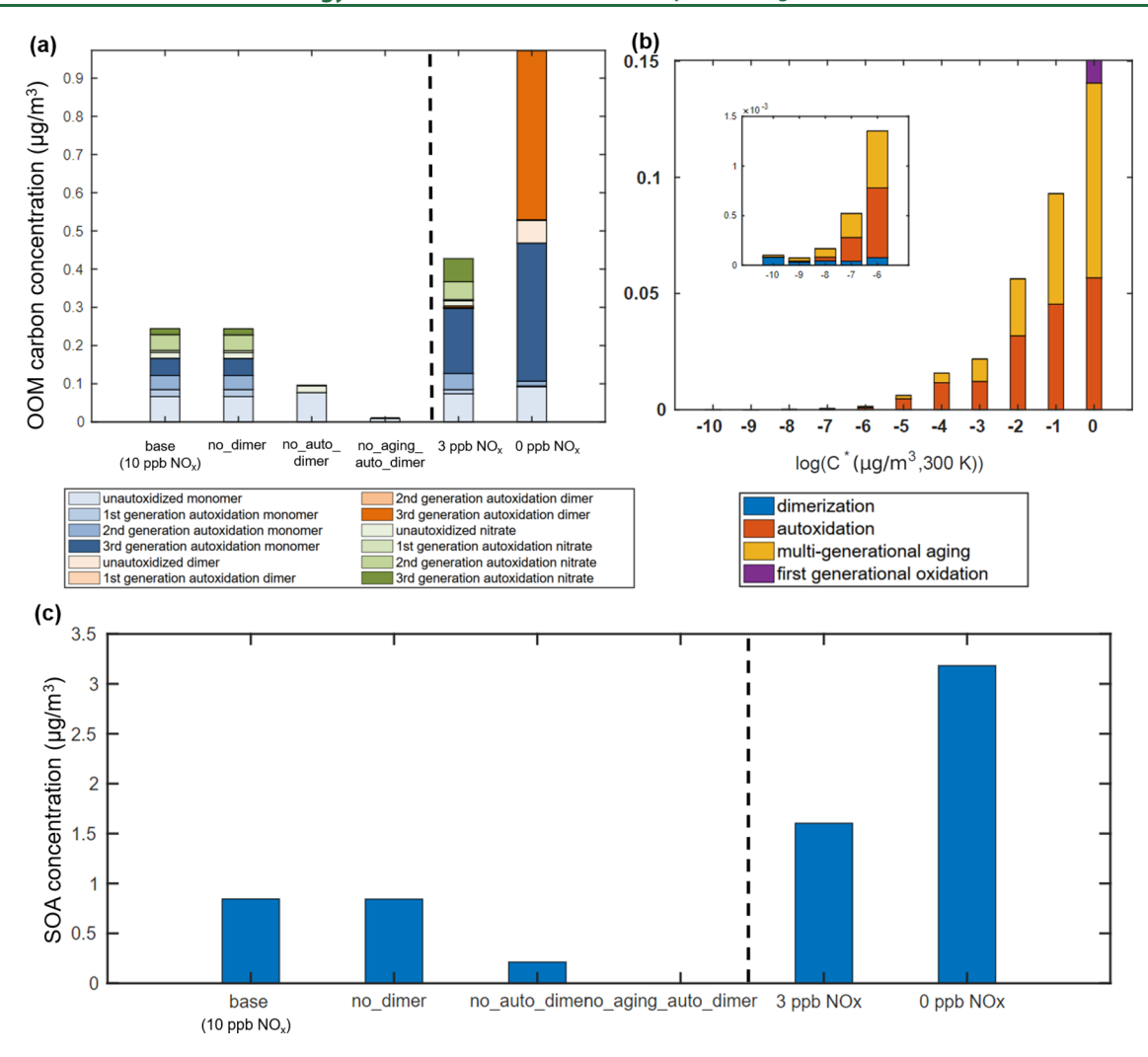


Figure 3. (a) OOM simulation concentrations in the base case as well as sensitivity cases that eliminate different reaction pathways or perturb NO_x concentrations, (b) the contributions of different reaction pathways to oxidation products with different volatilities, and (c) the same as panel (a) but for SOA concentrations.

pathways (dimerization, autoxidation, and multigenerational oxidation), NO_x (0 and 3 ppb), OH (5 × 10⁵ and 5 × 10⁶ #/cm³), precursor concentration (4.25 and 17 ppb in total), and temperature (270 and 310 K). The details of the sensitivity cases are shown in Section S10. The OOM and SOA concentrations of the base case and the sensitivity cases regarding the effects of reaction pathways and NO_x concentrations are shown in Figure 3a,c, and volatility distributions of OOMs of each case are shown in Figure S20. We also discuss the contribution of different reaction pathways to organic products with different volatilities, and the results are shown in Figure 3b.

In the base case, the concentrations of non-nitrogenous monomers and nitrates both have a significant contribution to the total concentration of the OOMs, while dimer concentration is neglectable. The volatility distribution of the OOMs shows that concentrations of non-nitrogenous monomers and nitrates decrease with decreasing volatility, while the dimer concentrations are higher in lower volatility bins. For products in $-4 \le \log C^* \le 0$ bins (LVOCs), the main contributors are unautoxidized non-nitrogenous monomers and organic nitrates. For products in $-8 \le \log C^* \le -5$ bins (ELVOCs), the main components are autoxidized non-nitrogenous monomers and nitrates. However, for products in $\log C^* \le -9$ bins

(ULVOCs), autoxidized dimers are the main contributors. In the first series of sensitivity cases ("no dimer", "no auto dimer", and "no aging auto dimer"), we evaluate the contributions of dimerization, autoxidation, and aging by sequentially turning off a reaction pathway based on the previous scenario. The contributions to products in the full volatility ranges from one pathway are the difference between two sensitivity cases with or without this pathway. For example, the dimer contributions are the difference between the "no dimer" and base cases. The total OOM and SOA concentrations in the "no dimer" scenario are almost the same as the base case, as the dimer concentration is low in the base case, though ULVOCs decrease substantially in the "no dimer" scenario. In the "no auto dimer" case, the concentrations of the OOMs and SOAs decrease by about 61 and 66% relative to the base case and the concentrations of ELVOCs decrease by about 70%, while those of the LVOCs decrease by about 60%. In the "no aging auto dimer" case, the OOM concentration is about 4% of the base case and there is no SOA generated; therefore, multigenerational aging can contribute to 20% of ELVOC formation and 40% of LVOC formation. Based on the results, autoxidation and multigenerational aging contribute approximately 61 and 35% of the concentration of the OOMs and 66 and 34% of the SOA

concentration, respectively, which means these processes are the two main contributors to the concentration of the OOM and SOA concentrations. The contributions to ELVOCs and LVOCs of autoxidation are higher than those of multigenerational oxidation, which means autoxidation contributes more to low-volatility products.

The second series of sensitivity cases are the same as the base case except that NO_x concentrations are set to 0 and 3 ppb (cf. 10 ppb in the base case), where 0 ppb represents a case without any NO_x effect and 3 ppb represents a lesspolluted case on clean days or under NO_x emission reduction in the future. The fraction of low-volatility products will increase when NO_x decreases, which induces an increase in the concentrations of the OOM and SOA concentrations. If the NO_x concentration decreases to 3 ppb, the concentrations of the OOMs and SOAs increase by about 60% relative to the base case. The increased OOMs are mainly autoxidized nonnitrogenous monomers and nitrates, while unautoxidized nonnitrogenous monomer and nitrate concentrations change slightly. The volatility distribution is similar to the base case, but the fractions of ELVOCs and ULVOCs increase due to the increase of autoxidized products. If the NOx effect is eliminated, then the concentrations of the OOMs and SOAs increase by about 200% compared to the base case, which is caused by increased concentrations of autoxidized nonnitrogenous monomers (mostly in the LVOC and ELVOC ranges) and autoxidized dimers (mostly in the ULVOC range). In this case, the fraction of low-volatility products greatly increases and ULVOCs can take up nearly half of total OOMs. The results of these two cases indicate that NO_x inhibits the generation of autoxidized products with low volatility. When NO_x emissions are abated, low-volatility OOMs, especially ULVOCs, could increase significantly.

In the third and fourth series of sensitivity cases, only OH and precursor concentrations are changed. Here, OOM and SOA concentrations vary almost linearly with OH and precursors (Figures S21 and S22). Product concentrations in the full volatility range also vary linearly with OH and precursors, but the compositions of OOMs are different under different OH concentrations. In the high OH case, the fractions of ULVOCs and ELVOCs to total OOMs are lower than the base case and low OH case, which may be caused by more unautoxidized products due to stronger multigenerational oxidation. Finally, in sensitivity cases where the temperature is changed (Figures S21 and S22), the concentration of the OOMs can vary by −25 and +20% at lower and higher temperatures, respectively, but the SOA concentration can vary by 100 and -20%. The low-volatility products decrease largely with decreased temperature. OOM formation, especially the formation of low-volatility products, is weaker at the lower temperature due to a lower autoxidation rate, but SOA concentrations increase with the decrease in temperature due to the influence of the gas-particle equilibrium. The OOMs and SOA changes can be explained similarly in the high-temperature case. We also discuss different temperature dependences of autoxidation at low and high temperatures, but the OOM and SOA concentrations and OOM volatility distribution only slightly change when temperature dependence changes.

4. ATMOSPHERIC IMPLICATIONS

In this study, we develop a novel model framework, I2D-VBS, for simulating the full volatility spectrum of products from the

benzene series of precursors. I2D-VBS traces molecular products and radicals and unifies multigenerational oxidation and irregular radical reaction in one framework. The model has been proven capable of simultaneously reproducing OOMs and SOA formation in experiments conducted using different precursor types (toluene, ethylbenzene, mesitylene, and xylene) under a wide range of precursor concentrations (50-800 ppb), OH exposure $(4 \times 10^8 - 8 \times 10^{11} \text{ cm}^{-3} \cdot \text{s})$, and NO_x concentrations (0–1000 ppb). The model also successfully reproduces the volatility and the O/C distributions of the OOMs in these experiments to the best of our knowledge for the first time, which sponsors the accuracy of the model in simulating the products over the full volatility range and enables a quantitative and holistic understanding of the formation mechanisms of these products. The simulated products over the full volatility range in I2D-VBS will help synchronize the formation of the OOMs and SOA and fill a large gap in the SOA formation, which is important for clarifying the formation processes and sources of SOA. Further, simulating the full volatility range of products, especially ELVOCs and LVOCs, can help simulate particle growth driven by organic condensation, which was significantly biased in previous models or observation-based calculations despite being important for accurately simulating CCN.

Moreover, the computational cost of I2D-VBS is deemed acceptable for three-dimensional (3D) simulation since it only introduces 10 new organic radical species compared to the traditional 2D-VBS, which has already been used in many 3D modeling studies. 50,64 For other precursors like monoterpenes and alkanes, we can also adjust parameters in the firstgenerational oxidation, radical reaction, and multigenerational oxidation modules by simulating experiments measuring OOMs and SOA to extend the model (see Section S11). The modest computational cost and extendibility guarantee the applicability of I2D-VBS to 3D chemical transport models (CTMs), and the accurate simulation of experiments measuring OOMs and SOA helps ensure the accuracy of atmospheric simulations. Hence, 3D CTMs with an I2D-VBS module can be used for predicting complex organic NPF, particle growth, cloud activation, and SOA formation processes worldwide, especially under the combined influence of climate change and emission reduction in the future.

ASSOCIATED CONTENT

Supporting Information

The Supporting Information is available free of charge at https://pubs.acs.org/doi/10.1021/acs.est.3c07128.

Comparison of simulated carbon yields by initial parameters of benzene series oxidation products with measured yields of OOMs; comparison of simulated SOA yields/concentrations and O/C with measurements conducted; model framework description; data calibration; experimental details; sensitivity simulation details and results (PDF)

AUTHOR INFORMATION

Corresponding Author

Bin Zhao — State Key Joint Laboratory of Environmental Simulation and Pollution Control, School of Environment, Tsinghua University, Beijing 100084, China; State Environmental Protection Key Laboratory of Sources and Control of Air Pollution Complex, Beijing 100084, China; orcid.org/0000-0001-8438-9188; Email: bzhao@mail.tsinghua.edu.cn

Authors

- Dejia Yin State Key Joint Laboratory of Environmental Simulation and Pollution Control, School of Environment, Tsinghua University, Beijing 100084, China; State Environmental Protection Key Laboratory of Sources and Control of Air Pollution Complex, Beijing 100084, China
- Shuxiao Wang State Key Joint Laboratory of Environmental Simulation and Pollution Control, School of Environment, Tsinghua University, Beijing 100084, China; State Environmental Protection Key Laboratory of Sources and Control of Air Pollution Complex, Beijing 100084, China; orcid.org/0000-0001-9727-1963
- Neil M. Donahue Center for Atmospheric Particle Studies, Carnegie Mellon University, Pittsburgh, Pennsylvania 15213, United States; © orcid.org/0000-0003-3054-2364
- Boyang Feng State Key Joint Laboratory of Environmental Simulation and Pollution Control, School of Environment, Tsinghua University, Beijing 100084, China; State Environmental Protection Key Laboratory of Sources and Control of Air Pollution Complex, Beijing 100084, China
- Xing Chang Laboratory of Transport Pollution Control and Monitoring Technology, Transport Planning and Research Institute, Ministry of Transport, Beijing 100028, China
- Qi Chen State Key Joint Laboratory of Environmental Simulation and Pollution Control, BIC-ESAT and IJRC, College of Environmental Sciences and Engineering, Peking University, Beijing 100871, China; orcid.org/0000-0003-3559-8914
- Xi Cheng State Key Joint Laboratory of Environmental Simulation and Pollution Control, BIC-ESAT and IJRC, College of Environmental Sciences and Engineering, Peking University, Beijing 100871, China
- Tengyu Liu Joint International Research Laboratory of Atmospheric and Earth System Sciences, School of Atmospheric Sciences, Nanjing University, Nanjing 210023, China; ⊚ orcid.org/0000-0002-3137-5898
- Chak K. Chan Division of Physical Sciences and Engineering, King Abdullah University of Science and Technology (KAUST), Thuwal 23955, Saudi Arabia; orcid.org/ 0000-0001-9687-8771
- Meredith Schervish Center for Atmospheric Particle Studies, Carnegie Mellon University, Pittsburgh, Pennsylvania 15213, United States; Department of Chemistry, University of California, Irvine, California 92697, United States; orcid.org/0009-0002-3365-9007
- Zeqi Li State Key Joint Laboratory of Environmental Simulation and Pollution Control, School of Environment, Tsinghua University, Beijing 100084, China; State Environmental Protection Key Laboratory of Sources and Control of Air Pollution Complex, Beijing 100084, China; orcid.org/0000-0003-3210-9310
- Yicong He State Key Joint Laboratory of Environmental Simulation and Pollution Control, School of Environment, Tsinghua University, Beijing 100084, China; State Environmental Protection Key Laboratory of Sources and Control of Air Pollution Complex, Beijing 100084, China
- Jiming Hao State Key Joint Laboratory of Environmental Simulation and Pollution Control, School of Environment, Tsinghua University, Beijing 100084, China; State

Environmental Protection Key Laboratory of Sources and Control of Air Pollution Complex, Beijing 100084, China

Complete contact information is available at: https://pubs.acs.org/10.1021/acs.est.3c07128

Notes

The authors declare no competing financial interest.

ACKNOWLEDGMENTS

This work was supported by the National Key R&D Program of China (2022YFC3700702), the National Natural Science Foundation of China (22188102 and 42275110), and the Samsung Advanced Institute of Technology. N.M.D. was supported by the National Science Foundation (CHE-2336463).

REFERENCES

- (1) IPCC Climate Change 2021: The Physical Science Basis. Contribution of Working Group I to the Sixth Assessment Report of the Intergovernmental Panel on Climate Change; Cambridge University Press: Cambridge, United Kingdom and New York, NY, USA, 2021.
- (2) Riipinen, I.; Pierce, J. R.; Yli-Juuti, T.; Nieminen, T.; Häkkinen, S.; Ehn, M.; Junninen, H.; Lehtipalo, K.; Petäjä, T.; Slowik, J.; Chang, R.; Shantz, N. C.; Abbatt, J.; Leaitch, W. R.; Kerminen, V. M.; Worsnop, D. R.; Pandis, S. N.; Donahue, N. M.; Kulmala, M. Organic condensation: a vital link connecting aerosol formation to cloud condensation nuclei (CCN) concentrations. *Atmos. Chem. Phys.* **2011**, *11* (8), 3865–3878.
- (3) Riipinen, I.; Yli-Juuti, T.; Pierce, J. R.; Petäjä, T.; Worsnop, D. R.; Kulmala, M.; Donahue, N. M. The contribution of organics to atmospheric nanoparticle growth. *Nat. Geosci.* **2012**, 5 (7), 453–458.
- (4) Kulmala, M.; Kerminen, V.-M. On the formation and growth of atmospheric nanoparticles. *Atmos. Res.* **2008**, *90* (2–4), 132–150.
- (5) Li, X.; Li, Y.; Cai, R.; Yan, C.; Qiao, X.; Guo, Y.; Deng, C.; Yin, R.; Chen, Y.; Li, Y.; Yao, L.; Sarnela, N.; Zhang, Y.; Petaja, T.; Bianchi, F.; Liu, Y.; Kulmala, M.; Hao, J.; Smith, J. N.; Jiang, J. Insufficient Condensable Organic Vapors Lead to Slow Growth of New Particles in an Urban Environment. *Environ. Sci. Technol.* 2022, 56 (14), 9936–9946.
- (6) Qiao, X.; Yan, C.; Li, X.; Guo, Y.; Yin, R.; Deng, C.; Li, C.; Nie, W.; Wang, M.; Cai, R.; Huang, D.; Wang, Z.; Yao, L.; Worsnop, D. R.; Bianchi, F.; Liu, Y.; Donahue, N. M.; Kulmala, M.; Jiang, J. Contribution of Atmospheric Oxygenated Organic Compounds to Particle Growth in an Urban Environment. *Environ. Sci. Technol.* 2021, 55 (20), 13646–13656.
- (7) Stolzenburg, D.; Fischer, L.; Vogel, A. L.; Heinritzi, M.; Schervish, M.; Simon, M.; Wagner, A. C.; Dada, L.; Ahonen, L. R.; Amorim, A.; Baccarini, A.; Bauer, P. S.; Baumgartner, B.; Bergen, A.; Bianchi, F.; Breitenlechner, M.; Brilke, S.; Buenrostro Mazon, S.; Chen, D.; Dias, A.; Draper, D. C.; Duplissy, J.; El Haddad, I.; Finkenzeller, H.; Frege, C.; Fuchs, C.; Garmash, O.; Gordon, H.; He, X.; Helm, J.; Hofbauer, V.; Hoyle, C. R.; Kim, C.; Kirkby, J.; Kontkanen, J.; Kurten, A.; Lampilahti, J.; Lawler, M.; Lehtipalo, K.; Leiminger, M.; Mai, H.; Mathot, S.; Mentler, B.; Molteni, U.; Nie, W.; Nieminen, T.; Nowak, J. B.; Ojdanic, A.; Onnela, A.; Passananti, M.; Petaja, T.; Quelever, L. L. J.; Rissanen, M. P.; Sarnela, N.; Schallhart, S.; Tauber, C.; Tome, A.; Wagner, R.; Wang, M.; Weitz, L.; Wimmer, D.; Xiao, M.; Yan, C.; Ye, P.; Zha, Q.; Baltensperger, U.; Curtius, J.; Dommen, J.; Flagan, R. C.; Kulmala, M.; Smith, J. N.; Worsnop, D. R.; Hansel, A.; Donahue, N. M.; Winkler, P. M. Rapid growth of organic aerosol nanoparticles over a wide tropospheric temperature range. Proc. Natl. Acad. Sci. U.S.A. 2018, 115 (37), 9122-9127.
- (8) Nie, W.; Yan, C.; Huang, D. D.; Wang, Z.; Liu, Y.; Qiao, X.; Guo, Y.; Tian, L.; Zheng, P.; Xu, Z.; Li, Y.; Xu, Z.; Qi, X.; Sun, P.; Wang, J.; Zheng, F.; Li, X.; Yin, R.; Dallenbach, K. R.; Bianchi, F.; Petäjä, T.; Zhang, Y.; Wang, M.; Schervish, M.; Wang, S.; Qiao, L.; Wang, Q.; Zhou, M.; Wang, H.; Yu, C.; Yao, D.; Guo, H.; Ye, P.; Lee,

- S.; Li, Y. J.; Liu, Y.; Chi, X.; Kerminen, V.-M.; Ehn, M.; Donahue, N. M.; Wang, T.; Huang, C.; Kulmala, M.; Worsnop, D.; Jiang, J.; Ding, A. Secondary organic aerosol formed by condensing anthropogenic vapours over China's megacities. Nat. Geosci. 2022, 15 (4), 255-261. (9) Gordon, H.; Sengupta, K.; Rap, A.; Duplissy, J.; Frege, C.; Williamson, C.; Heinritzi, M.; Simon, M.; Yan, C.; Almeida, J.; Tröstl, J.; Nieminen, T.; Ortega, I. K.; Wagner, R.; Dunne, E. M.; Adamov, A.; Amorim, A.; Bernhammer, A.-K.; Bianchi, F.; Breitenlechner, M.; Brilke, S.; Chen, X.; Craven, J. S.; Dias, A.; Ehrhart, S.; Fischer, L.; Flagan, R. C.; Franchin, A.; Fuchs, C.; Guida, R.; Hakala, J.; Hoyle, C. R.; Jokinen, T.; Junninen, H.; Kangasluoma, J.; Kim, J.; Kirkby, J.; Krapf, M.; Kürten, A.; Laaksonen, A.; Lehtipalo, K.; Makhmutov, V.; Mathot, S.; Molteni, U.; Monks, S. A.; Onnela, A.; Peräkylä, O.; Piel, F.; Petäjä, T.; Praplan, A. P.; Pringle, K. J.; Richards, N. A. D.; Rissanen, M. P.; Rondo, L.; Sarnela, N.; Schobesberger, S.; Scott, C. E.; Seinfeld, J. H.; Sharma, S.; Sipilä, M.; Steiner, G.; Stozhkov, Y.; Stratmann, F.; Tomé, A.; Virtanen, A.; Vogel, A. L.; Wagner, A. C.; Wagner, P. E.; Weingartner, E.; Wimmer, D.; Winkler, P. M.; Ye, P.; Zhang, X.; Hansel, A.; Dommen, J.; Donahue, N. M.; Worsnop, D. R.; Baltensperger, U.; Kulmala, M.; Curtius, J.; Carslaw, K. S. Reduced anthropogenic aerosol radiative forcing caused by biogenic new particle formation. Proc. Natl. Acad. Sci. U.S.A. 2016, 113 (43), 12053-12058.
- (10) Kirkby, J.; Duplissy, J.; Sengupta, K.; Frege, C.; Gordon, H.; Williamson, C.; Heinritzi, M.; Simon, M.; Yan, C.; Almeida, J.; Trostl, J.; Nieminen, T.; Ortega, I. K.; Wagner, R.; Adamov, A.; Amorim, A.; Bernhammer, A. K.; Bianchi, F.; Breitenlechner, M.; Brilke, S.; Chen, X.; Craven, J.; Dias, A.; Ehrhart, S.; Flagan, R. C.; Franchin, A.; Fuchs, C.; Guida, R.; Hakala, J.; Hoyle, C. R.; Jokinen, T.; Junninen, H.; Kangasluoma, J.; Kim, J.; Krapf, M.; Kurten, A.; Laaksonen, A.; Lehtipalo, K.; Makhmutov, V.; Mathot, S.; Molteni, U.; Onnela, A.; Perakyla, O.; Piel, F.; Petaja, T.; Praplan, A. P.; Pringle, K.; Rap, A.; Richards, N. A.; Riipinen, I.; Rissanen, M. P.; Rondo, L.; Sarnela, N.; Schobesberger, S.; Scott, C. E.; Seinfeld, J. H.; Sipila, M.; Steiner, G.; Stozhkov, Y.; Stratmann, F.; Tome, A.; Virtanen, A.; Vogel, A. L.; Wagner, A. C.; Wagner, P. E.; Weingartner, E.; Wimmer, D.; Winkler, P. M.; Ye, P.; Zhang, X.; Hansel, A.; Dommen, J.; Donahue, N. M.; Worsnop, D. R.; Baltensperger, U.; Kulmala, M.; Carslaw, K. S.; Curtius, J. Ion-induced nucleation of pure biogenic particles. Nature **2016**, 533 (7604), 521–526.
- (11) Ehn, M.; Thornton, J. A.; Kleist, E.; Sipila, M.; Junninen, H.; Pullinen, I.; Springer, M.; Rubach, F.; Tillmann, R.; Lee, B.; Lopez-Hilfiker, F.; Andres, S.; Acir, I. H.; Rissanen, M.; Jokinen, T.; Schobesberger, S.; Kangasluoma, J.; Kontkanen, J.; Nieminen, T.; Kurten, T.; Nielsen, L. B.; Jorgensen, S.; Kjaergaard, H. G.; Canagaratna, M.; Maso, M. D.; Berndt, T.; Petaja, T.; Wahner, A.; Kerminen, V. M.; Kulmala, M.; Worsnop, D. R.; Wildt, J.; Mentel, T. F. A large source of low-volatility secondary organic aerosol. *Nature* 2014, 506 (7489), 476–479.
- (12) Schervish, M.; Donahue, N. M. Peroxy radical chemistry and the volatility basis set. *Atmos. Chem. Phys.* **2020**, 20 (2), 1183–1199. (13) Bianchi, F.; Kurten, T.; Riva, M.; Mohr, C.; Rissanen, M. P.; Roldin, P.; Berndt, T.; Crounse, J. D.; Wennberg, P. O.; Mentel, T. F.; Wildt, J.; Junninen, H.; Jokinen, T.; Kulmala, M.; Worsnop, D. R.; Thornton, J. A.; Donahue, N.; Kjaergaard, H. G.; Ehn, M. Highly Oxygenated Organic Molecules (HOM) from Gas-Phase Autoxidation Involving Peroxy Radicals: A Key Contributor to Atmospheric Aerosol. *Chem. Rev.* **2019**, *119* (6), 3472–3509.
- (14) Roldin, P.; Ehn, M.; Kurten, T.; Olenius, T.; Rissanen, M. P.; Sarnela, N.; Elm, J.; Rantala, P.; Hao, L.; Hyttinen, N.; Heikkinen, L.; Worsnop, D. R.; Pichelstorfer, L.; Xavier, C.; Clusius, P.; Ostrom, E.; Petaja, T.; Kulmala, M.; Vehkamaki, H.; Virtanen, A.; Riipinen, I.; Boy, M. The role of highly oxygenated organic molecules in the Boreal aerosol-cloud-climate system. *Nat. Commun.* **2019**, *10* (1), No. 4370.
- (15) Mohr, C.; Thornton, J. A.; Heitto, A.; Lopez-Hilfiker, F. D.; Lutz, A.; Riipinen, I.; Hong, J.; Donahue, N. M.; Hallquist, M.; Petaja, T.; Kulmala, M.; Yli-Juuti, T. Molecular identification of organic

- vapors driving atmospheric nanoparticle growth. Nat. Commun. 2019, 10 (1), No. 4442.
- (16) Tröstl, J.; Chuang, W. K.; Gordon, H.; Heinritzi, M.; Yan, C.; Molteni, U.; Ahlm, L.; Frege, C.; Bianchi, F.; Wagner, R.; Simon, M.; Lehtipalo, K.; Williamson, C.; Craven, J. S.; Duplissy, J.; Adamov, A.; Almeida, J.; Bernhammer, A. K.; Breitenlechner, M.; Brilke, S.; Dias, A.; Ehrhart, S.; Flagan, R. C.; Franchin, A.; Fuchs, C.; Guida, R.; Gysel, M.; Hansel, A.; Hoyle, C. R.; Jokinen, T.; Junninen, H.; Kangasluoma, J.; Keskinen, H.; Kim, J.; Krapf, M.; Kurten, A.; Laaksonen, A.; Lawler, M.; Leiminger, M.; Mathot, S.; Mohler, O.; Nieminen, T.; Onnela, A.; Petaja, T.; Piel, F. M.; Miettinen, P.; Rissanen, M. P.; Rondo, L.; Sarnela, N.; Schobesberger, S.; Sengupta, K.; Sipila, M.; Smith, J. N.; Steiner, G.; Tome, A.; Virtanen, A.; Wagner, A. C.; Weingartner, E.; Wimmer, D.; Winkler, P. M.; Ye, P.; Carslaw, K. S.; Curtius, J.; Dommen, J.; Kirkby, J.; Kulmala, M.; Riipinen, I.; Worsnop, D. R.; Donahue, N. M.; Baltensperger, U. The role of low-volatility organic compounds in initial particle growth in the atmosphere. Nature 2016, 533 (7604), 527-531.
- (17) Coggon, M. M.; Gkatzelis, G. I.; McDonald, B. C.; Gilman, J. B.; Schwantes, R. H.; Abuhassan, N.; Aikin, K. C.; Arend, M. F.; Berkoff, T. A.; Brown, S. S.; Campos, T. L.; Dickerson, R. R.; Gronoff, G.; Hurley, J. F.; Isaacman-VanWertz, G.; Koss, A. R.; Li, M.; McKeen, S. A.; Moshary, F.; Peischl, J.; Pospisilova, V.; Ren, X.; Wilson, A.; Wu, Y.; Trainer, M.; Warneke, C. Volatile chemical product emissions enhance ozone and modulate urban chemistry. *Proc. Natl. Acad. Sci. U.S.A.* 2021, 118 (32), No. e2026653118, DOI: 10.1073/pnas.2026653118.
- (18) Qiao, X.; Li, X.; Yan, C.; Sarnela, N.; Yin, R.; Guo, Y.; Yao, L.; Nie, W.; Huang, D.; Wang, Z.; Bianchi, F.; Liu, Y.; Donahue, N. M.; Kulmala, M.; Jiang, J. Precursor apportionment of atmospheric oxygenated organic molecules using a machine learning method. *Environ. Sci.: Atmos.* **2023**, *3* (1), 230–237.
- (19) Tian, L.; Huang, D. D.; Wang, Q.; Zhu, S.; Wang, Q.; Yan, C.; Nie, W.; Wang, Z.; Qiao, L.; Liu, Y.; Qiao, X.; Guo, Y.; Zheng, P.; Jing, S.; Lou, S.; Wang, H.; Yu, J. Z.; Huang, C.; Li, Y. J. Underestimated Contribution of Heavy Aromatics to Secondary Organic Aerosol Revealed by Comparative Assessments Using New and Traditional Methods. ACS Earth Space Chem. 2023, 7 (1), 110–119.
- (20) Wang, Y.; Clusius, P.; Yan, C.; Dallenbach, K.; Yin, R.; Wang, M.; He, X. C.; Chu, B.; Lu, Y.; Dada, L.; Kangasluoma, J.; Rantala, P.; Deng, C.; Lin, Z.; Wang, W.; Yao, L.; Fan, X.; Du, W.; Cai, J.; Heikkinen, L.; Tham, Y. J.; Zha, Q.; Ling, Z.; Junninen, H.; Petaja, T.; Ge, M.; Wang, Y.; He, H.; Worsnop, D. R.; Kerminen, V. M.; Bianchi, F.; Wang, L.; Jiang, J.; Liu, Y.; Boy, M.; Ehn, M.; Donahue, N. M.; Kulmala, M. Molecular Composition of Oxygenated Organic Molecules and Their Contributions to Organic Aerosol in Beijing. *Environ. Sci. Technol.* **2022**, *56* (2), 770–778.
- (21) Wang, Y.; Mehra, A.; Krechmer, J. E.; Yang, G.; Hu, X.; Lu, Y.; Lambe, A.; Canagaratna, M.; Chen, J.; Worsnop, D.; Coe, H.; Wang, L. Oxygenated products formed from OH-initiated reactions of trimethylbenzene: autoxidation and accretion. *Atmos. Chem. Phys.* **2020**, *20* (15), 9563–9579.
- (22) Xu, L.; Møller, K. H.; Crounse, J. D.; Kjaergaard, H. G.; Wennberg, P. O. New Insights into the Radical Chemistry and Product Distribution in the OH-Initiated Oxidation of Benzene. *Environ. Sci. Technol.* **2020**, *54* (21), 13467–13477.
- (23) Wang, S.; Wu, R.; Berndt, T.; Ehn, M.; Wang, L. Formation of Highly Oxidized Radicals and Multifunctional Products from the Atmospheric Oxidation of Alkylbenzenes. *Environ. Sci. Technol.* **2017**, *51* (15), 8442–8449.
- (24) Cheng, X.; Chen, Q.; Jie Li, Y.; Zheng, Y.; Liao, K.; Huang, G. Highly oxygenated organic molecules produced by the oxidation of benzene and toluene in a wide range of OH exposure and NO_x conditions. *Atmos. Chem. Phys.* **2021**, 21 (15), 12005–12019.
- (25) Wang, M.; Chen, D.; Xiao, M.; Ye, Q.; Stolzenburg, D.; Hofbauer, V.; Ye, P.; Vogel, A. L.; Mauldin, R. L., 3rd; Amorim, A.; Baccarini, A.; Baumgartner, B.; Brilke, S.; Dada, L.; Dias, A.; Duplissy, J.; Finkenzeller, H.; Garmash, O.; He, X. C.; Hoyle, C. R.; Kim, C.;

- Kvashnin, A.; Lehtipalo, K.; Fischer, L.; Molteni, U.; Petaja, T.; Pospisilova, V.; Quelever, L. L. J.; Rissanen, M.; Simon, M.; Tauber, C.; Tome, A.; Wagner, A. C.; Weitz, L.; Volkamer, R.; Winkler, P. M.; Kirkby, J.; Worsnop, D. R.; Kulmala, M.; Baltensperger, U.; Dommen, J.; El-Haddad, I.; Donahue, N. M. Photo-oxidation of Aromatic Hydrocarbons Produces Low-Volatility Organic Compounds. *Environ. Sci. Technol.* **2020**, *54* (13), 7911–7921.
- (26) Carter, W. P. L. Development of the SAPRC-07 chemical mechanism. *Atmos. Environ.* **2010**, 44 (40), 5324–5335.
- (27) Stockwell, W. R.; Saunders, E.; Goliff, W. S.; Fitzgerald, R. M. A perspective on the development of gas-phase chemical mechanisms for Eulerian air quality models. *J. Air Waste Manage. Assoc.* **2020**, *70* (1), 44–70.
- (28) Jenkin, M. E.; Saunders, S. M.; Wagner, V.; Pilling, M. J. Protocol for the development of the Master Chemical Mechanism, MCM v3 (Part B): tropospheric degradation of aromatic volatile organic compounds. *Atmos. Chem. Phys.* **2003**, 3 (1), 181–193.
- (29) Donahue, N. M.; Epstein, S. A.; Pandis, S. N.; Robinson, A. L. A two-dimensional volatility basis set: 1. organic-aerosol mixing thermodynamics. *Atmos. Chem. Phys.* **2011**, *11* (7), 3303–3318.
- (30) Donahue, N. M.; Henry, K. M.; Mentel, T. F.; Kiendler-Scharr, A.; Spindler, C.; Bohn, B.; Brauers, T.; Dorn, H. P.; Fuchs, H.; Tillmann, R.; Wahner, A.; Saathoff, H.; Naumann, K. H.; Mohler, O.; Leisner, T.; Muller, L.; Reinnig, M. C.; Hoffmann, T.; Salo, K.; Hallquist, M.; Frosch, M.; Bilde, M.; Tritscher, T.; Barmet, P.; Praplan, A. P.; DeCarlo, P. F.; Dommen, J.; Prevot, A. S.; Baltensperger, U. Aging of biogenic secondary organic aerosol via gas-phase OH radical reactions. *Proc. Natl. Acad. Sci. U.S.A.* 2012, 109 (34), 13503–13508.
- (31) Donahue, N. M.; Kroll, J. H.; Pandis, S. N.; Robinson, A. L. A two-dimensional volatility basis set Part 2: Diagnostics of organicaerosol evolution. *Atmos. Chem. Phys.* **2012**, *12* (2), *615*–*634*.
- (32) Zhao, B.; Wang, S.; Donahue, N. M.; Chuang, W.; Hildebrandt Ruiz, L.; Ng, N. L.; Wang, Y.; Hao, J. Evaluation of one-dimensional and two-dimensional volatility basis sets in simulating the aging of secondary organic aerosol with smog-chamber experiments. *Environ. Sci. Technol.* **2015**, 49 (4), 2245–2254.
- (33) Chuang, W. K.; Donahue, N. M. A two-dimensional volatility basis set Part 3: Prognostic modeling and NO_x dependence. *Atmos. Chem. Phys.* **2016**, *16* (1), 123–134.
- (34) Schervish, M.; Donahue, N. M. Peroxy radical kinetics and new particle formation. *Environ. Sci.: Atmos.* **2021**, *1* (2), 79–92.
- (35) Atkinson, R.; Carter, W. P. L.; Plum, C. N.; Winer, A. M.; Pitts, J. N., Jr. Kinetics of the gas-phase reactions of NO3 radicals with a series of aromatics at 296 ± 2 K. Int. J. Chem. Kinet. 1984, 16 (7), 887-898.
- (36) Tomas, A.; Olariu, R. I.; Barnes, I.; Becker, K. H. Kinetics of the reaction of O3 with selected benzenediols. *Int. J. Chem. Kinet.* **2003**, 35 (6), 223–230.
- (37) Birdsall, A. W.; Elrod, M. J. Comprehensive NO-dependent study of the products of the oxidation of atmospherically relevant aromatic compounds. *J. Phys. Chem. A* **2011**, *115* (21), 5397–5407.
- (38) Li, Y.; Wang, L. The atmospheric oxidation mechanism of 1,2,4-trimethylbenzene initiated by OH radicals. *Phys. Chem. Chem. Phys.* **2014**, *16* (33), 17908–17917.
- (39) Nishino, N.; Arey, J.; Atkinson, R. Formation Yields of Glyoxal and Methylglyoxal from the Gas-Phase OH Radical-Initiated Reactions of Toluene, Xylenes, and Trimethylbenzenes as a Function of NO2 Concentration. *J. Phys. Chem. A* **2010**, *114* (37), 10140–10147.
- (40) Pankow, J. F.; Asher, W. E. SIMPOL.1: a simple group contribution method for predicting vapor pressures and enthalpies of vaporization of multifunctional organic compounds. *Atmos. Chem. Phys.* **2008**, *8* (10), 2773–2796.
- (41) Wu, R.; Pan, S.; Li, Y.; Wang, L. Atmospheric oxidation mechanism of toluene. *J. Phys. Chem. A* **2014**, *118* (25), 4533–4547. (42) Zaytsev, A.; Koss, A. R.; Breitenlechner, M.; Krechmer, J. E.; Nihill, K. J.; Lim, C. Y.; Rowe, J. C.; Cox, J. L.; Moss, J.; Roscioli, J. R.; Canagaratna, M. R.; Worsnop, D. R.; Kroll, J. H.; Keutsch, F. N.

- Mechanistic study of the formation of ring-retaining and ring-opening products from the oxidation of aromatic compounds under urban atmospheric conditions. *Atmos. Chem. Phys.* **2019**, *19* (23), 15117–15129.
- (43) Berndt, T.; Scholz, W.; Mentler, B.; Fischer, L.; Herrmann, H.; Kulmala, M.; Hansel, A. Accretion Product Formation from Self- and Cross-Reactions of RO(2) Radicals in the Atmosphere. *Angew. Chem., Int. Ed.* **2018**, *57* (14), 3820–3824.
- (44) Molteni, U.; Bianchi, F.; Klein, F.; El Haddad, I.; Frege, C.; Rossi, M. J.; Dommen, J.; Baltensperger, U. Formation of highly oxygenated organic molecules from aromatic compounds. *Atmos. Chem. Phys.* **2018**, *18* (3), 1909–1921.
- (45) Jenkin, M. E.; Valorso, R.; Aumont, B.; Rickard, A. R. Estimation of rate coefficients and branching ratios for reactions of organic peroxy radicals for use in automated mechanism construction. *Atmos. Chem. Phys.* **2019**, *19* (11), 7691–7717.
- (46) Bloss, C.; Wagner, V.; Jenkin, M. E.; Volkamer, R.; Bloss, W. J.; Lee, J. D.; Heard, D. E.; Wirtz, K.; Martin-Reviejo, M.; Rea, G.; Wenger, J. C.; Pilling, M. J. Development of a detailed chemical mechanism (MCMv3.1) for the atmospheric oxidation of aromatic hydrocarbons. *Atmos. Chem. Phys.* **2005**, *5* (3), 641–664.
- (47) Tsiligiannis, E.; Hammes, J.; Salvador, C. M.; Mentel, T. F.; Hallquist, M. Effect of NO_x on 1,3,5-trimethylbenzene (TMB) oxidation product distribution and particle formation. *Atmos. Chem. Phys.* **2019**, 19 (23), 15073–15086.
- (48) Bates, K. H.; Jacob, D. J.; Li, K.; Ivatt, P. D.; Evans, M. J.; Yan, Y.; Lin, J. Development and evaluation of a new compact mechanism for aromatic oxidation in atmospheric models. *Atmos. Chem. Phys.* **2021**, *21* (24), 18351–18374.
- (49) Pye, H. O. T.; Place, B. K.; Murphy, B. N.; Seltzer, K. M.; D'Ambro, E. L.; Allen, C.; Piletic, I. R.; Farrell, S.; Schwantes, R. H.; Coggon, M. M.; Saunders, E.; Xu, L.; Sarwar, G.; Hutzell, W. T.; Foley, K. M.; Pouliot, G.; Bash, J.; Stockwell, W. R. Linking gas, particulate, and toxic endpoints to air emissions in the Community Regional Atmospheric Chemistry Multiphase Mechanism (CRACMM). Atmos. Chem. Phys. 2023, 23 (9), 5043–5099.
- (50) Zhao, B.; Wang, S.; Donahue, N. M.; Jathar, S. H.; Huang, X.; Wu, W.; Hao, J.; Robinson, A. L. Quantifying the effect of organic aerosol aging and intermediate-volatility emissions on regional-scale aerosol pollution in China. *Sci. Rep* **2016**, *6*, No. 28815.
- (51) Mao, J.; Ren, X.; Brune, W. H.; Olson, J. R.; Crawford, J. H.; Fried, A.; Huey, L. G.; Cohen, R. C.; Heikes, B.; Singh, H. B.; Blake, D. R.; Sachse, G. W.; Diskin, G. S.; Hall, S. R.; Shetter, R. E. Airborne measurement of OH reactivity during INTEX-B. *Atmos. Chem. Phys.* **2009**, 9 (1), 163–173.
- (52) Liu, T.; Huang, D. D.; Li, Z.; Liu, Q.; Chan, M.; Chan, C. K. Comparison of secondary organic aerosol formation from toluene on initially wet and dry ammonium sulfate particles at moderate relative humidity. *Atmos. Chem. Phys.* **2018**, *18* (8), 5677–5689.
- (53) Ruiz, L. H.; Paciga, A. L.; Cerully, K. M.; Nenes, A.; Donahue, N. M.; Pandis, S. N. Formation and aging of secondary organic aerosol from toluene: changes in chemical composition, volatility, and hygroscopicity. *Atmos. Chem. Phys.* **2015**, *15* (14), 8301–8313.
- (54) Bian, Q.; May, A. A.; Kreidenweis, S. M.; Pierce, J. R. Investigation of particle and vapor wall-loss effects on controlled wood-smoke smog-chamber experiments. *Atmos. Chem. Phys.* **2015**, 15 (19), 11027–11045.
- (55) He, Y.; King, B.; Pothier, M.; Lewane, L.; Akherati, A.; Mattila, J.; Farmer, D. K.; McCormick, R. L.; Thornton, M.; Pierce, J. R.; Volckens, J.; Jathar, S. H. Secondary organic aerosol formation from evaporated biofuels: comparison to gasoline and correction for vapor wall losses. *Environ. Sci.: Processess Impacts* **2020**, 22 (7), 1461–1474.
- (56) Berndt, T. Peroxy Radical Processes and Product Formation in the OH Radical-Initiated Oxidation of alpha-Pinene for Near-Atmospheric Conditions. *J. Phys. Chem. A* **2021**, *125* (41), 9151–9160.
- (57) Berndt, T. Peroxy Radical and Product Formation in the Gas-Phase Ozonolysis of alpha-Pinene under Near-Atmospheric Conditions: Occurrence of an Additional Series of Peroxy Radicals O,O-

- C(10)H(15)O(O(2))(y)O(2) with y = 1-3. J. Phys. Chem. A 2022, 126 (37), 6526-6537.
- (58) He, Y.; Akherati, A.; Nah, T.; Ng, N. L.; Garofalo, L. A.; Farmer, D. K.; Shiraiwa, M.; Zaveri, R. A.; Cappa, C. D.; Pierce, J. R.; Jathar, S. H. Particle Size Distribution Dynamics Can Help Constrain the Phase State of Secondary Organic Aerosol. *Environ. Sci. Technol.* **2021**, 55 (3), 1466–1476.
- (59) He, Y.; Lambe, A. T.; Seinfeld, J. H.; Cappa, C. D.; Pierce, J. R.; Jathar, S. H. Process-Level Modeling Can Simultaneously Explain Secondary Organic Aerosol Evolution in Chambers and Flow Reactors. *Environ. Sci. Technol.* **2022**, *56* (10), 6262–6273.
- (60) Hodzic, A.; Madronich, S.; Kasibhatla, P. S.; Tyndall, G.; Aumont, B.; Jimenez, J. L.; Lee-Taylor, J.; Orlando, J. Organic photolysis reactions in tropospheric aerosols: effect on secondary organic aerosol formation and lifetime. *Atmos. Chem. Phys.* **2015**, *15* (16), 9253–9269.
- (61) Kang, E.; Root, M. J.; Toohey, D. W.; Brune, W. H. Introducing the concept of Potential Aerosol Mass (PAM). *Atmos. Chem. Phys.* **2007**, 7 (22), 5727–5744.
- (62) China Ministry of Ecological Environment China Ecological Environment Status Bulletin. 2018.
- (63) Cui, L.; Wu, D.; Wang, S.; Xu, Q.; Hu, R.; Hao, J. Measurement report: Ambient volatile organic compound (VOC) pollution in urban Beijing: characteristics, sources, and implications for pollution control. *Atmos. Chem. Phys.* **2022**, 22 (18), 11931–11944.
- (64) Chang, X.; Zheng, H.; Zhao, B.; Yan, C.; Jiang, Y.; Hu, R.; Song, S.; Dong, Z.; Li, S.; Li, Z.; Zhu, Y.; Shi, H.; Jiang, Z.; Xing, J.; Wang, S. Drivers of High Concentrations of Secondary Organic Aerosols in Northern China during the COVID-19 Lockdowns. *Environ. Sci. Technol.* **2023**, *57* (14), 5521–5531.